nature photonics

LETTERS

PUBLISHED ONLINE: 18 APRIL 2016 | DOI: 10.1038/NPHOTON.2016.74

Frequency-domain Hong–Ou–Mandel interference

Toshiki Kobayashi[1], Rikizo Ikuta[1], Shuto Yasui[1], Shigehito Miki[2], Taro Yamashita[2], Hirotaka Terai[2], Takashi Yamamoto[1], Masato Koashi[3] and Nobuyuki Imoto[1]*

Hong–Ou–Mandel (HOM) interference is one of the most prominent features of quantum indistinguishable particles, and has been used as the core of many quantum information protocols[1]. Since its first observation in 1987[2], it has been understood as a phenomenon that occurs when two identical bosons are fed to two input ports of a beam splitter. Here, we report the observation of HOM interference exhibited by two photons with different colours[3]. We developed a frequency-domain beam splitter via a second-order nonlinear medium driven by strong coherent light[4,5]. A photon passing through the device changes its colour probabilistically. When a single pulse containing two photons with different colours was fed to the beam splitter, the pair of output photons showed a tendency to assume the same colour, with a visibility exceeding the classical limit. Combined with wavelength-division multiplexing, our results will pave the way towards the miniaturization of highly integrated optical circuits for quantum information processing.

The applications of HOM interference in quantum information processing are diversifying, including quantum computation[6–9], quantum key distribution[10,11], quantum repeaters[12–14] and quantum-optical coherence tomography[15]. HOM interference has been observed with photons generated not only from spontaneous parametric down-conversion (SPDC)[2] but also from quantum dots[16,17], trapped neutral atoms[18], trapped ions[19], nitrogen–vacancy centres[20] and silicon–vacancy centres[21] in diamond. Furthermore, bosonic particles other than photons—for example, surface plasmons[22,23], helium-4 atoms[24] and phonons[25]—also show HOM interference. Although the repertoire of physical systems that exhibit HOM interference has been steadily growing, to the best of our knowledge, all of them essentially used a spatial or polarization beam splitter (BS), which is a static device. Replacing it with a dynamical device will extend the realm into other degrees of freedom, such as frequency or energy. In contrast to polarization, the frequency degree of freedom has the potential for multiplexing many modes into a single spatial mode, and has been attracting much attention[26,27]. It has been proposed that a frequency conversion in a nonlinear optical media[28–30] could be used as a frequency-domain BS for HOM interference[3].

We first introduce HOM interference between the photons with different frequencies via a partial frequency converter based on the second-order nonlinear optical effect[3]. Suppose that an upper angular frequency ω_s, a lower angular frequency ω_i and an angular frequency ω_p of the pump light satisfy $\omega_i = \omega_s - \omega_p$, as shown in Fig. 1a. When the pump light is sufficiently strong, the effective Hamiltonian of the nonlinear optical process is described by

$$\hat{H} = i\hbar\left(g^{*}\hat{a}_i^{\dagger}\hat{a}_s - g\hat{a}_i\hat{a}_s^{\dagger}\right) \tag{1}$$

where $\hat{a}_{s(i)}$ and $\hat{a}_{s(i)}^{\dagger}$ are annihilation and creation operators of the upper (lower) frequency modes. $g = |g|e^{i\phi}$ is proportional to the complex amplitude of the pump light, where ϕ represents the phase of the pump light[29,31]. g^{*} is the complex conjugate of g. Using equation (1), annihilation operators $\hat{a}_{s,out}$ and $\hat{a}_{i,out}$ of the signal and the idler modes from the nonlinear optical medium are described by

$$\hat{a}_{s,out} = \cos(|g|\tau)\hat{a}_s - e^{i\phi}\sin(|g|\tau)\hat{a}_i \tag{2}$$

and

$$\hat{a}_{i,out} = e^{-i\phi}\sin(|g|\tau)\hat{a}_s + \cos(|g|\tau)\hat{a}_i \tag{3}$$

where τ is the travelling time of the light pulses through the nonlinear optical medium. The probability of a photon staying in the same input frequency mode is given by $\cos^2(|g|\tau)$ and the transition probability of the photon from an input frequency mode to the other frequency mode is $\sin^2(|g|\tau)$. The process of frequency conversion described in equations (2) and (3) can be seen as a BS with two different frequency input (output) modes[3–5]. Borrowing the terminology of the spatial BS, we may regard $\cos^2(|g|\tau)$ and $\sin^2(|g|\tau)$ as the transmittance and the reflectance, respectively.

In the frequency converter, the transition probability can be adjusted by changing the pump power. When we choose the pump power such that $\cos^2(|g|\tau) = \sin^2(|g|\tau) = 1/2$, the frequency converter works as a half BS acting on the two frequency modes. In such a situation, when a single photon in the upper mode and another single photon in the lower mode are injected into the frequency converter simultaneously, the two photons never exit in different frequency modes, but always in the same frequency modes. This phenomenon is a precise analogue of HOM interference in the frequency degree of freedom. One may wonder why, unlike the conventional HOM experiments, two distinct bosons that are distinguished by their frequencies show HOM interference. As shown in Fig. 1b, however, the crux of HOM interference is the destructive interference between the output events. Therefore, what is really required in the process is indistinguishability after the frequency conversion, which can be fulfilled by a suitable coherent property of the converter.

The experimental set-up for frequency-domain HOM interference using a partial frequency converter is shown in Fig. 1c. We prepare a vertically (V) polarized heralded single photon at 780 nm in mode A. In mode B, instead of a single photon, we prepare a V-polarized weak laser pulse at 1,522 nm with average photon number of $\mu \sim 0.1$ (see Methods). The pulse contains multiphotons at a probability of $O(\mu^2)$, but it is dominated by the desired single-photon events occurring at $O(\mu)$ given the heralding signal[32,33]. Note that use of laser pulses for both input modes results the desired events decreasing to $O(\mu^2)$ and the visibility will never exceed 0.5,

[1]Graduate School of Engineering Science, Osaka University, Toyonaka, Osaka 560-8531, Japan. [2]Advanced ICT Research Institute, National Institute of Information and Communications Technology (NICT), Kobe 651-2492, Japan. [3]Photon Science Center, Graduate School of Engineering, The University of Tokyo, Bunkyo-ku, Tokyo 113-8656, Japan. *e-mail: imoto@mp.es.osaka-u.ac.jp

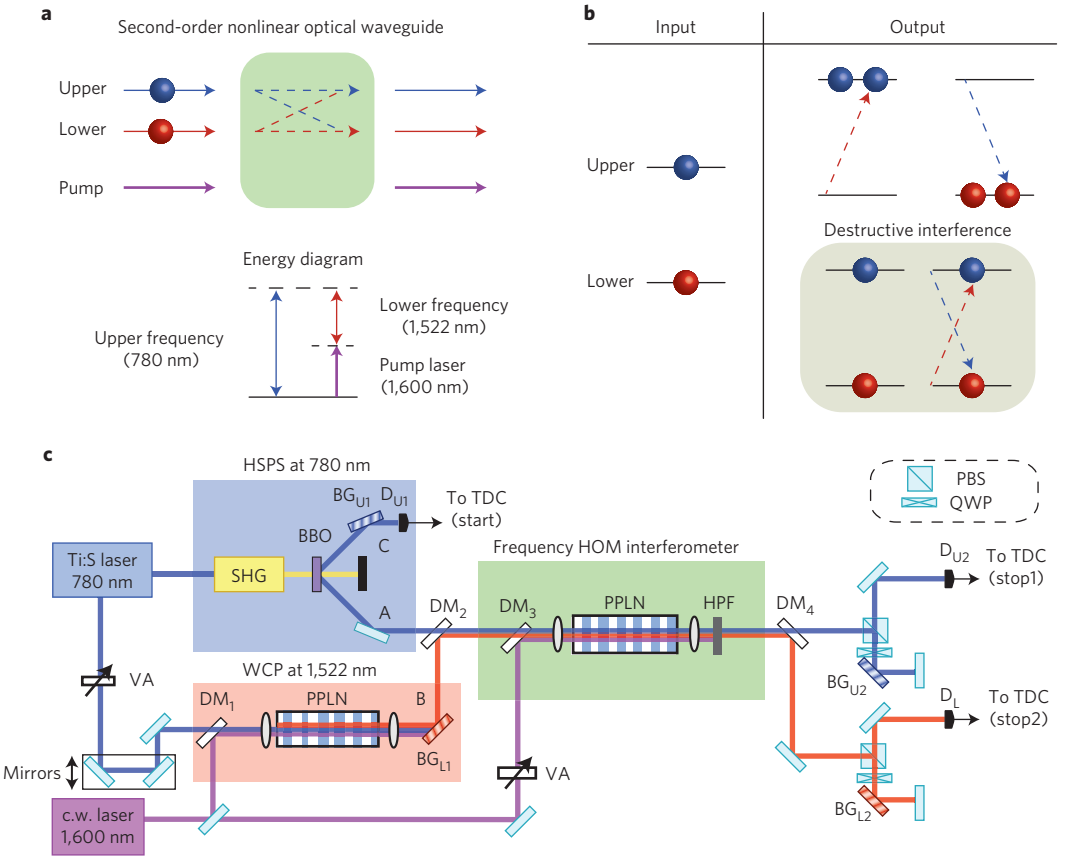

Figure 1 | Frequency-domain HOM interferometer. a, The frequency converter based on the second-order nonlinear optical effect. It partially converts the wavelengths of the photons in a single spatial mode from/to 780 nm to/from 1,522 nm via difference/sum frequency generation. **b**, Principle of the frequency-domain HOM effect. When a single photon in the upper mode and another photon in the lower mode are mixed by the frequency converter, the single photon occupation events in the output disappear due to the destructive interference. **c**, The experimental set-up for frequency-domain HOM interference. In the experiment, the heralded single photon source (HSPS) at 780 nm and the weak coherent pulse (WCP) at 1,522 nm are prepared to serve as two input photons to the frequency HOM interferometer. The two photons are combined by DM_2 into a single spatial mode and then enter the PPLN waveguide used as the frequency-domain BS. The output light pulses are separated into two spatial modes by DM_4 for photon detection of the two frequency modes. BBO, β-barium borate; HPF, high-pass filter; PBS, polarizing beam splitter; QWP, quarter-wave plate; TDC, time-to-digital converter.

as the classical wave theory predicts. The two light pulses are combined by a dichroic mirror (DM_2) and then focused on a type-0 quasi-phase-matched periodically poled $LiNbO_3$ (PPLN) waveguide[29] for the frequency conversion. The time difference between the two light pulses is adjusted by mirrors on a motorized stage. The V-polarized continuous wave (c.w.) pump laser at 1,600 nm is combined with the two input light pulses by DM_3 and focused on the PPLN waveguide. The length of the PPLN crystal is 20 mm and the acceptable bandwidth is calculated to be $\Delta_{WG} \equiv 140$ GHz. The pump power is adjusted by a variable attenuator (VA) and determines the transition probability of the frequency converter.

After the frequency converter, the light pulses at 780 nm and 1,522 nm are separated by DM_4 and Bragg gratings (BG_{U2} and BG_{L2} with bandwidths of $\Delta_U \equiv 99$ GHz and $\Delta_L \equiv 130$ GHz, respectively). They are then measured by an avalanche photodiode with a quantum efficiency of about 60% for 780-nm photons (D_{U2}) and by a superconducting single-photon detector (SSPD)[34] with a quantum efficiency of about 60% for the 1,522-nm photons (D_L), respectively. To observe HOM interference, we collect the threefold coincidence events among the three detectors D_{U1}, D_{U2} and D_L. Note that SSPD with a quantum efficiency of about 30% for 780-nm photons (D_{U1}) is used for heralding the 780-nm input photon in mode A.

Before demonstrating frequency-domain HOM interference, we first measured the dependencies of the count rates of the transition/staying events $p_{U,t/s}$ and $p_{L,t/s}$ on the pump power for the upper and the lower input photons, respectively. The experimental result is shown in Fig. 2a,b. We estimate the internal transition probability R of the frequency converter, which depends on the pump power P and the frequency of the input light, by constructing a theoretical model as follows.

We assume that the internal transition probability $R = R(P, \omega)$ is a Gaussian with the bandwidth of Δ_{WG} around the centre of 780/1,522 nm for upper/lower input light, at which the peak value is given by $\tilde{R}(P)$. We also assume that the optical circuit for frequency-domain HOM interference after preparing the single photon and the coherent light pulse is decomposed to a lossless frequency converter with a transition probability of $R(P, \omega)$ and a staying probability of $T(P, \omega)(=1 - R(P, \omega))$, two lossy media inducing the loss in the upper and the lower input modes and two spectral filters acting on the two output modes. The transmittances of the lossy media for the upper and the lower input light, which describe the optical loss including the insertion loss to the frequency converter, are denoted by $T_{in,U}$ and $T_{in,L}$, respectively. The transmittances of the spectral filters for the upper and the lower output light, which describe the optical loss including the BGs after the frequency converter and the quantum efficiencies of the detectors, are denoted by $T_{out,U}(\omega)$ and $T_{out,L}(\omega)$, respectively. We assume that the transmittance $T_{out,U/L}(\omega)$ is Gaussian with a peak value of $\tilde{T}_{out,U/L}$. The bandwidths of $T_{out,U}(\omega)$ and $T_{out,L}(\omega)$ are calculated to be 70 and 92 GHz, respectively, due to BG_{U2} and BG_{L2} being used twice. For

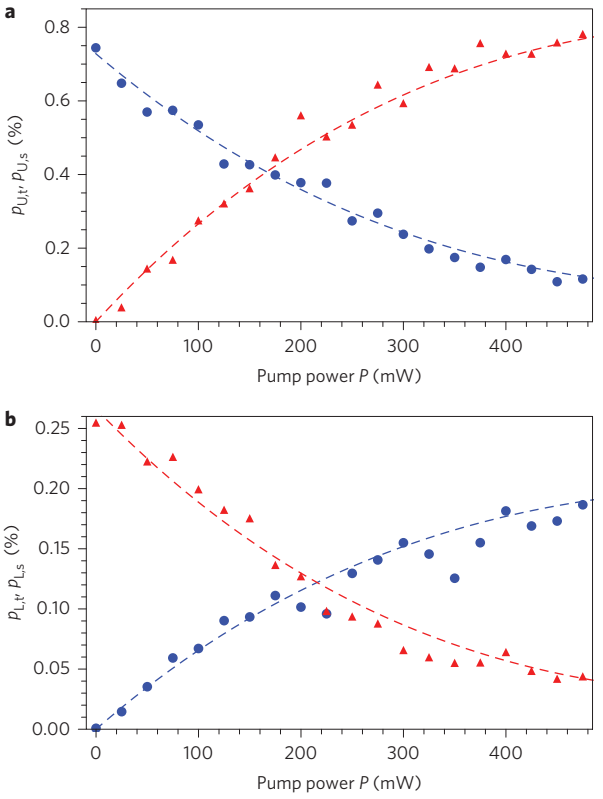

Figure 2 | The count rate versus the pump power. a, The count rate of the transition/staying events per pulse $p_{U,t/s}$ (circle/triangle) for the heralded single photon at 780 nm when the heralding signal is detected at D_{V1}. **b**, The count rate of the transition/staying events per pulse $p_{L,t/s}$ (triangle/circle) for the coherent light pulse at 1,522 nm. The dashed curves are obtained from our theoretical model with the observed values of $p_{U,t/s}$ and $p_{L,t/s}$ (see Supplementary Information).

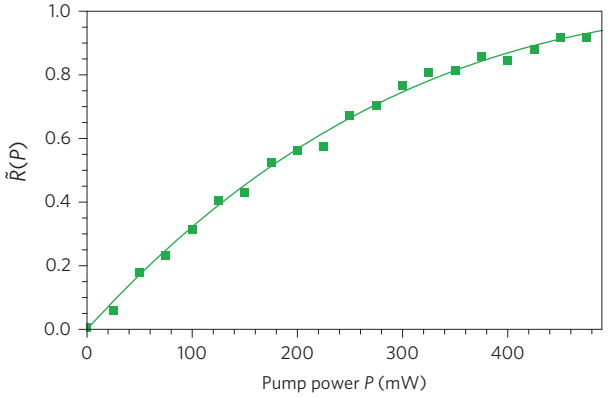

Figure 3 | The peak value of the internal transition probability. The curve is obtained by the best fit to $\tilde{R}(P)$ with $A\sin^2(\sqrt{\eta P})$, where the fitting parameters A and η are 0.99 and 0.0036 per mW, respectively.

the input light pulses, we assume that the spectral shapes of the heralded single photon and the coherent light pulse are Gaussian with bandwidths of 740 and 93 GHz, respectively. These are calculated using the experimental parameters Δ_{WG}, Δ_U and Δ_L and the pulse width of the laser source $\Delta t \equiv 1.2$ ps. The emission rate of the photon pair from SPDC is so small that multiple-pair events are negligible. In addition, the heralded genuine single photon is assumed to be in a pure state because the narrow-band spectral filtering destroys the spectral correlation between the photon pair from SPDC. Under these assumptions, the initial state composed of the single photon and the coherent state is regarded as a pure state described by $|\phi\rangle = \hat{a}_U^\dagger \hat{D}_L(\alpha)|0\rangle$, where $\hat{a}_U^\dagger$ is a creation operator of the upper mode, $\hat{D}_L(\alpha)$ is a displacement operator with complex number α of the lower mode and $|0\rangle$ is the vacuum state for both modes. On the basis of the above theoretical model with the use of the observed values $p_{U,t}(P)$, $p_{U,s}(P)$, $p_{L,t}(P)$ and $p_{L,s}(P)$, we calculated $\tilde{R}(P)$, $T_{in,U}\tilde{T}_{out,U}$, $T_{in,U}\tilde{T}_{out,L}$ and $|\alpha|^2 T_{in,L}/T_{in,U}$ for various values of P (see Supplementary Information). The result for $\tilde{R}(P)$ is shown in Fig. 3.

Next we demonstrated frequency-domain HOM interference by using the frequency converter. We set the pump power to be 140 mW, which results in a transition probability of ~0.4 of the frequency converter according to Fig. 3. The experimental result of the dependency of the threefold coincidence counts on the optical delay is shown in Fig. 4a. The observed visibility of 0.71 ± 0.04 at the zero delay point was obtained by the best fit to the experimental data with a Gaussian. The full width at the half maximum was approximately 1.7 mm, which corresponds to a delay time of ~6 ps. The high visibility clearly shows nonclassical HOM interference between the two light pulses in a single spatial mode with different frequencies. We also measured the visibilities at pump powers of 50 and 290 mW, which correspond to transition probabilities of ~0.2 and ~0.7, respectively. The experimental results are shown in Fig. 4b. The observed visibilities are 0.34 ± 0.10 at 50 mW and 0.65 ± 0.10 at 290 mW.

In the following, we discuss the reasons for the degradation of the visibility. In our theoretical model, we can calculate the visibility by using the experimental parameters $\tilde{R}(P_0)$, $T_{in,U}\tilde{T}_{out,U}$, $T_{in,U}\tilde{T}_{out,L}$ and $|\alpha|^2 T_{in,L}/T_{in,U}$ (see Supplementary Information), the results of which are the dashed curves shown in Fig. 4a,b. These are in good agreement with the experimental results. Figure 4b indicates that the highest visibility of 0.81 will be obtained when the pump power is 190 mW, which corresponds to a transition probability of ~0.5. In our theoretical model, the main reasons for the degradation of the visibility are due to the input light pulses, namely, the effect of the multiphoton components in the coherent light pulse at 1,522 nm and the broad bandwidth of the heralded single photon at 780 nm. If we replace the coherent light pulse by a single photon and set $T_{in,L}$ to be equal to $T_{in,U}$, the visibility of HOM interference is expected to be 0.95 at a pump ower of 190 mW. If we use the single photon at 780 nm with the same bandwidth as that of the coherent light pulse, the visibility will be 0.93 at 190 mW, and if we assume both of these improvements for the input light pulses, the visibility will be 0.98 at 190 mW.

In conclusion, we have demonstrated frequency-domain HOM interference between a heralded single photon at 780 nm and weak laser light at 1,522 nm in a single spatial mode by using a partial frequency converter based on the nonlinear optical effect. We also deduced that the performance of the demonstrated frequency-domain HOM interferometer is close to ideal from the fact that the estimated visibility in the case of the ideal input photons is 0.98, which is close to unity. The spatial HOM interferometer has already been exploited in a wide variety of quantum phenomena including large-scale quantum information processing. We thus believe that the frequency-domain HOM interferometer will open up new frequency-domain quantum interferometry and provide a tool for exploiting quantum phenomena and a way of scaling up quantum information processing with a large Hilbert space spanned by multiple frequency modes.

Methods

Methods and any associated references are available in the online version of the paper.

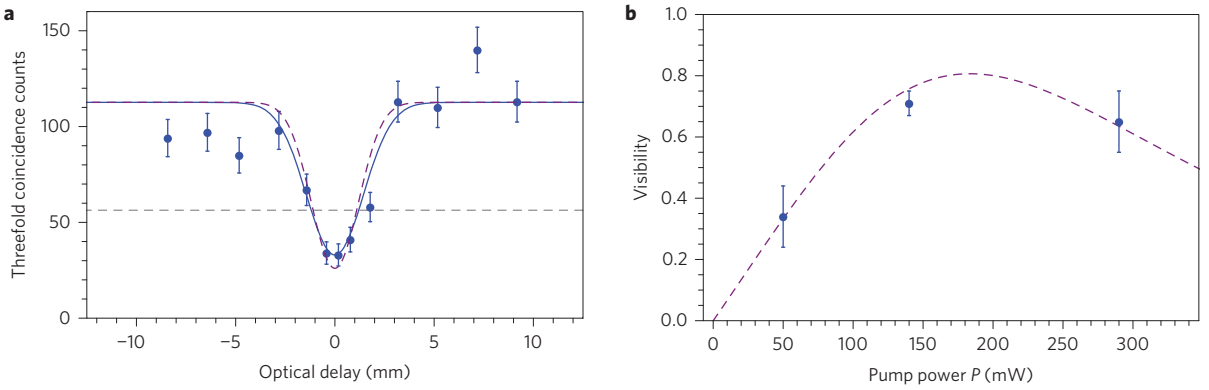

Figure 4 | Observed frequency-domain HOM interference. a, The observed HOM dip at 140 mW pump power. The circles represent the experimental threefold coincidence counts. The solid curve is the Gaussian fit to the experimental counts. The dashed curve is obtained from our theoretical model under the experimental parameters. The dashed horizontal line describes the half value of the maximum of the fitting result. **b**, The dependence of the visibility on pump power. The circles represent the experimental results. The dashed curve is obtained from our theoretical model under the experimental parameters. The error bars indicate the standard deviations estimated by Monte Carlo method under the assumption of the Poisson statistics of the photon counts.

Received 24 December 2015; accepted 16 March 2016; published online 18 April 2016

References

1. Pan, J.-W. *et al.* Multiphoton entanglement and interferometry. *Rev. Mod. Phys.* **84,** 777–838 (2012).
2. Hong, C. K., Ou, Z. Y. & Mandel, L. Measurement of subpicosecond time intervals between two photons by interference. *Phys. Rev. Lett.* **59,** 2044–2046 (1987).
3. Raymer, M., van Enk, S., McKinstrie, C. & McGuinness, H. Interference of two photons of different color. *Opt. Commun.* **283,** 747–752 (2010).
4. Giorgi, G., Mataloni, P. & De Martini, F. Frequency hopping in quantum interferometry: efficient up-down conversion for qubits and ebits. *Phys. Rev. Lett.* **90,** 027902 (2003).
5. Ikuta, R. *et al.* Observation of two output light pulses from a partial wavelength converter preserving phase of an input light at a single-photon level. *Opt. Express* **21,** 27865–27872 (2013).
6. Kok, P. *et al.* Linear optical quantum computing with photonic qubits. *Rev. Mod. Phys.* **79,** 135–174 (2007).
7. Barz, S. *et al.* Demonstration of blind quantum computing. *Science* **335,** 303–308 (2012).
8. Spagnolo, N. *et al.* Experimental validation of photonic boson sampling. *Nature Photon.* **8,** 615–620 (2014).
9. Carolan, J. *et al.* Universal linear optics. *Science* **349,** 711–716 (2015).
10. Tang, Y.-L. *et al.* Measurement-device-independent quantum key distribution over 200 km. *Phys. Rev. Lett.* **113,** 190501 (2014).
11. Guan, J.-Y. *et al.* Experimental passive round-robin differential phase-shift quantum key distribution. *Phys. Rev. Lett.* **114,** 180502 (2015).
12. Sangouard, N., Simon, C., de Riedmatten, H. & Gisin, N. Quantum repeaters based on atomic ensembles and linear optics. *Rev. Mod. Phys.* **83,** 33–80 (2011).
13. Hofmann, J. *et al.* Heralded entanglement between widely separated atoms. *Science* **337,** 72–75 (2012).
14. Bao, X.-H. *et al.* Quantum teleportation between remote atomic-ensemble quantum memories. *Proc Natl Acad. Sci. USA* **109,** 20347–20351 (2012).
15. Teich, M., Saleh, B., Wong, F. & Shapiro, J. Variations on the theme of quantum optical coherence tomography: a review. *Quantum Inf. Process.* **11,** 903–923 (2012).
16. Santori, C., Fattal, D., Vuckovic, J., Solomon, G. S. & Yamamoto, Y. Indistinguishable photons from a single-photon device. *Nature* **419,** 594–597 (2002).
17. Patel, R. B. *et al.* Two-photon interference of the emission from electrically tunable remote quantum dots. *Nature Photon.* **4,** 632–635 (2010).
18. Beugnon, J. *et al.* Quantum interference between two single photons emitted by independently trapped atoms. *Nature* **440,** 779–782 (2006).
19. Maunz, P. *et al.* Quantum interference of photon pairs from two remote trapped atomic ions. *Nature Phys.* **3,** 538–541 (2007).
20. Sipahigil, A. *et al.* Quantum interference of single photons from remote nitrogen-vacancy centers in diamond. *Phys. Rev. Lett.* **108,** 143601 (2012).
21. Sipahigil, A. *et al.* Indistinguishable photons from separated silicon-vacancy centers in diamond. *Phys. Rev. Lett.* **113,** 113602 (2014).
22. Di Martino, G. *et al.*Observation of quantum interference in the plasmonic Hong–Ou–Mandel effect. *Phys. Rev. Appl.* **1,** 034004 (2014).
23. Fakonas, J. S., Lee, H., Kelaita, Y. A. & Atwater, H. A. Two-plasmon quantum interference. *Nature Photon.* **8,** 317–320 (2014).
24. Lopes, R. *et al.* Atomic Hong–Ou–Mandel experiment. *Nature* **520,** 66–68 (2015).
25. Toyoda, K., Hiji, R., Noguchi, A. & Urabe, S. Hong–Ou–Mandel interference of two phonons in trapped ions. *Nature* **527,** 74–77 (2015).
26. Shih, Y. H. & Sergienko,, A. V. Observation of quantum beating in a simple beam-splitting experiment: Two-particle entanglement in spin and space-time. *Phys. Rev. A* **50,** 2564 (1994).
27. Ramelow, S. Ratschbacher, L. Fedrizzi, A. Langford, N. K. & Zeilinger, A. Discrete tunable color entanglement. *Phys. Rev. Lett.* **103,** 253601 (2009).
28. Tanzilli, S. *et al.* A photonic quantum information interface. *Nature* **437,** 116–120 (2005).
29. Ikuta, R. *et al.* Wide-band quantum interface for visible-to-telecommunication wavelength conversion. *Nature Commun.* **2,** 537 (2011).
30. Ikuta, R. *et al.* High-fidelity conversion of photonic quantum information to telecommunication wavelength with superconducting single-photon detectors. *Phys. Rev. A* **87,** 010301(R) (2013).
31. Kumar, P. Quantum frequency conversion. *Opt. Lett.* **15,** 1476–1478 (1990).
32. Rarity, J. G., Tapster, P. R. & Loudon, R. Non-classical interference between independent sources. *J. Opt. B* **7,** S171 (2005).
33. Ikuta, R. *et al.* Nonclassical two-photon interference between independent telecommunication light pulses converted by difference-frequency generation. *Phys. Rev. A* **88,** 042317 (2013).
34. Miki, S., Yamashita, T., Terai, H. & Wang, Z. High performance fiber-coupled NbTiN superconducting nanowire single photon detectors with Gifford-McMahon cryocooler. *Opt. Express* **21,** 10208–10214 (2013).

Acknowledgements

This work was supported by a Japan Society for the Promotion of Science (JSPS) Grant-in-Aid for JSPS Fellows (Grant No. 14J04677) and MEXT/JSPS KAKENHI Grant Nos 25247068, 15H03704, 15KK0164 and 25286077.

Author contributions

T.K., R.I and T.Y. designed the experiment. T.K., R.I and S.Y. carried out the experiments under supervision of T.Y., M.K. and N.I. S.M., T.Y. and H.T. developed the system of the superconducting single-photon detectors. All authors analysed the experimental results and contributed to the discussions and interpretations. T.K. wrote the manuscript, with input from all authors.

Additional information

Supplementary information is available in the online version of the paper. Reprints and permissions information is available online at www.nature.com/reprints. Correspondence and requests for materials should be addressed to N.I.

Competing financial interests

The authors declare no competing financial interests.

Methods

Preparation of the two input light pulses. A light pulse from a mode-locked Ti:sapphire laser at 780 nm (pulse width $\Delta t \equiv 1.2$ ps; repetition rate of 82 MHz) is used for the preparation. It is divided into two beams. One beam is used to prepare a heralded single photon at 780 nm. The beam is frequency-doubled (wavelength: 390 nm; power: 200 mW) by second-harmonic generation, and then pumps a type-I phase-matched 1.5-mm-thick β-barium borate (BBO) crystal to generate a photon pair at 780 nm in modes A and C through SPDC. The photon in mode C is measured by D_{U1}, which prepares a heralded single photon in mode A. The spectral filtering of the photon in mode C is performed by BG_{U1} with a bandwidth of $\Delta_U \equiv 99$ GHz, which corresponds to 0.2 nm for 780 nm light.

The other beam from the Ti:S laser is used to prepare the weak coherent light pulse at 1,522 nm. The beam enters a difference frequency generation (DFG) module. In the DFG module, a V-polarized cw pump laser at 1,600 nm is combined with the input light pulse at 780 nm by DM_1. They are focused on a type-0 quasi-phase-matched PPLN waveguide[29]. The PPLN waveguide consists of Zn-doped lithium niobate as the waveguide core and lithium tantalite as the cladding layer. The length of the PPLN crystal is 20 mm and the acceptable bandwidth is calculated to be $\Delta_{WG} = 140$ GHz, which corresponds to 0.28 nm for 780 nm light and 1.1 nm for 1,522 nm light. After passing through the PPLN waveguide, the converted light at 1,522 nm is extracted by BG_{L1} with a bandwidth of $\Delta_L \equiv 130$ GHz, which corresponds to 1 nm for 1,522 nm light. We adjust the average photon number of the coherent light pulse at 1,522 nm to ~0.1 using a VA.